INSTITUTE OF PHYSICS PUBLISHING NONLINEARITY

Nonlinearity **18** (2005) 609–630 doi:10.1088/0951-7715/18/2/009

On degenerate saturated-diffusion equations with convection

Alina Chertock[1], **Alexander Kurganov**[2] **and Philip Rosenau**[3]

[1] Department of Mathematics, North Carolina State University, Raleigh, NC 27695, USA
[2] Mathematics Department, Tulane University, New Orleans, LA 70118, USA
[3] School of Mathematical Sciences, Tel-Aviv University, Tel-Aviv 69978, Israel

E-mail: chertock@math.ncsu.edu, kurganov@math.tulane.edu and rosenau@post.tau.ac.il

Received 8 June 2004, in final form 4 October 2004
Published 6 December 2004
Online at stacks.iop.org/Non/18/609

Recommended by R Krasny

Abstract

We study a class of degenerate parabolic convection–diffusion equations, endowed with a mechanism for saturation of the diffusion flux, which corrects the unphysical gradient-flux relations at high gradients. This paper extends our previous works on the effects of diffusion with saturation on convection and the impact of saturation on porous media-type diffusion, where it has been demonstrated that a nonlinear saturating diffusion is susceptible to a self-induced formation of discontinuities. In this work we demonstrate that nonlinear convection enhances the breakdown effect. We carry both analytical and numerical studies of the model equation, $u_t + f(u)_x = [\varphi(u)Q(u_x, u)]_x$, where Q is a bounded increasing function, $\varphi(0) = 0$ and $\varphi(u) \sim u^n$, $n > 0$ for $u \sim 0$. Depending on a choice of n, we obtain two distinctive processes. If $0 \leqslant n \leqslant 1$, a discontinuity forms only when the upstream–downstream disparity exceeds a critical threshold, but if $n > 1$, *all travelling waves are found to have a sharp discontinuous front*. In fact, given a compact or a semi-compact initial datum, the front will not start to move until such a discontinuity forms.

Mathematics Subject Classification: 35K65, 35B65, 35K55, 35B40

(Some figures in this article are in colour only in the electronic version)

1. Introduction

In this paper we are mainly concerned with the model equation

$$u_t + f(u)_x = [\varphi(u)Q(u_x)]_x, \tag{1.1}$$

subject to a non-negative initial datum

$$u(x,0) = u_0(x). \tag{1.2}$$

Here f, Q and φ are smooth functions, satisfying $Q'(s) > 0 \,\forall\, s$, $|Q(s)| < Q_\infty$, $Q(0) = 0$; $\varphi'(u) \geqslant 0$ for $u \geqslant 0$, $\varphi(0) = 0$ and $\varphi(u) \sim u^n$, $n > 0$ for $u \sim 0$ (an alternative model equation with $Q = (\ln u)_x$ is briefly discussed in section 4.2).

This degenerate parabolic convection–diffusion equation may be thought of as an extension of the Burgers equation with a built-in mechanism that takes into account the fact that in real physical processes the dissipative flux saturates at high gradients. This work extends our previous studies of a saturation mechanism being imposed on *linear diffusion* [7, 11, 17, 18].

A typical example of Q is

$$Q(s) = \frac{s}{\sqrt{1+s^2}}, \tag{1.3}$$

which also corresponds to a mean-curvature-type diffusion flux. Of course, for the linear flux case, wherein $Q \sim u_x$, the problem reduces to the classical extension of the Burgers equation due to the Fick law (or the Fourier law) diffusion flux:

$$u_t + f(u)_x = [\varphi(u)u_x]_x.$$

The particulars of the chosen dissipative flux were discussed in our earlier works. Here we would like to remind the reader that though the boundedness of the flux function Q, which is a fundamental property of real physical systems, is almost always lost in the small gradient expansions underlying the derivation of most, if not all, continuum models and since in real processes the exact form of the diffusion is rarely, if ever, known, there is a certain arbitrariness in the choice of the saturating flux function Q. The synthesized form of the assumed diffusion flux is in a sense a Padé approximant, which interpolates between the universal forms characterizing the dissipative process in both *very small* and *very large gradients*. Typically, insofar as Q is monotonic in gradients and saturates at a proper rate, the behaviour of the flux function at gradients of order one is to a large extent of secondary importance.

The model equation, studied in this paper, unifies into one equation our previous works where, while studying the impact of saturated diffusion, we either ignored convection altogether and thus studied

$$u_t = [u^n Q(u_x)]_x, \qquad n \geqslant 0, \tag{1.4}$$

or, using equation (1.4) with $n = 0$, appended it with convection to obtain Burgers-type equations of the form

$$u_t + f(u)_x = [Q(u_x)]_x. \tag{1.5}$$

When $n = 0$, equation (1.4) reveals that if the flux saturation rate is sufficiently large, the resolution of initially imposed discontinuities is delayed [5, 18]. Equation (1.4) with $n > 0$ is recognized as the porous medium equation with an embedded saturation mechanism. We have recently found [7] that for $n > 1$ the parabolic degeneracy may cause a *self-induced formation of discontinuities* out of the continuous initial datum as opposed to the classical porous medium equation ((1.4) with a linear $Q(u_x) = u_x$), where sharp but continuous fronts typically form (see, e.g. [1–4, 6, 9]).

Equation (1.5) was proposed in [16] and later studied in [8, 11, 19]. As one may expect, nonlinear convection enhances the conditions for a breakdown. In fact, the most interesting feature of (1.5) is the effect of criticality, that is, unlike small amplitude solutions that remain smooth at all times, *large amplitude solutions may develop discontinuities*. This feature is

easily seen via the analysis of travelling waves (TW) [11, 16]: while small amplitude kinks are smooth, in large amplitude kinks part of the upstream–downstream transition must be accomplished via a discontinuous jump (*subshocks*). Thus induced discontinuities may persist indefinitely since the TWs represent a forced motion. Unlike the classical Burgers case, here, due to the saturation of fluxes, the viscous forces have a bounded range. When the inertial forcing exceeds a certain threshold, the disparity between the inertial and dissipative forces is resolved by the formation of a discontinuity.

We would like to stress the fundamental difference between the formation of discontinuities as a self-propelling effect in (1.4) with $n > 1$, and the convection–diffusion case (1.5), where the breakdown is stimulated by the nonlinear convection. In the former case, with a compactly supported initial datum, the sharp front is due to the following competing processes: diffusion spreads the mass from the inner parts of the domain towards the fronts, which are kept immobile due to the the saturation mechanism. This causes the mass to 'pile-up' at the outer edges of the domain and continues until 'overpiling' is about to occur. To circumvent this catastrophe *a sharp discontinuity forms and begins to move*. In appendix A, we exemplify these effects in the two-dimensional case, where we also show that though different parts of the initial front may start moving at different times ultimately, a universal, axisymmetric pattern is attained. On the other hand, when the solution is only considered on a finite time interval, there may not be enough time to converge to isotropy. This possibility is explored in the second example, where an initial-boundary value problem is studied numerically. Due to anisotropic initial conditions, an initially given circular hole deforms and the cavity collapses into a slit. Though numerical constraints allow us to follow that process only up to a finite stages of the collapse, if one normalizes the y-size of the cavity, then the numerics reveals that the width shrinks at an approximately constant rate. A further discussion of this fascinating phenomenon will be given elsewhere.

In the model presented in the main part of the paper, we append the saturation mechanisms present in (1.4) with nonlinear convection which hastens the formation of a discontinuity and thus the initiation of the front's motion. Given the fact that our model introduces sharp discontinuities, one could ask: how does the present model improve the description of the underlying phenomena? When answering that question it is important to realize that the effects of saturation are both microscopic and macroscopic. Clearly, whenever a shock discontinuity emerges in our model, apart from calling attention to its existence, we cannot say much about the underlying structure (this, of course, would necessitate a microscopic description of the layer). However, our study can be viewed as a meaningful step forwards since it calls attention to other mechanisms that will intervene in the dynamics, whenever our model predicts a discontinuity (something you would never know in the conventional description). Yet, other consequences of diffusion saturation are macroscopic, like an initial delay in propagation or thinning of the shock layer. This is a true and measurable effect that we are able to capture. Thus, where the conventional diffusion smeared completely, our ability to peek into the high gradient zone provides us with macroscopic consequences of the impact of the saturation on the overall dynamics.

Our main results may be summarized as follows.

- A TW analysis of equation (1.1) with $f(u) \sim u^m$, $\varphi(u) \sim u^n$, for $u \sim 0$ reveals that:
  (1) If $0 < n \leqslant 1$, the effects of criticality are the same as in the $n = 0$ case.
  (2) If $n > 1$, then *no continuous TW solutions with* $U(-\infty) > 0$ *and* $U(\infty) = 0$ *are possible.*

  We also demonstrate numerically that both the continuous and the discontinuous TWs *are strong attractors for a wide class of appropriate initial data.*

- We show that 'small' positive solutions remain smooth.
- Our main theoretical result is a finite-time breakdown of the 'large' semi-compact solutions of equation (1.1) with $\varphi(u) = u$. We recall that for $n > 1$, the occurrence of the breakdown is obvious, because, even without the presence of convection, the solution develops discontinuities. However, for $0 < n \leqslant 1$, the situation is not so obvious. At this point we can prove only the $n = 1$ case, which seems to be a border value between different patterns. Our proof is an extension of the breakdown proof of [8], though the employed assumptions are different. We firmly believe that the breakdown of 'large' solutions occurs in the $0 < n < 1$ case as well, but we still lack a rigorous proof.
- We also study the behaviour of 'small' and 'large' compactly supported solutions. For $n \leqslant 1$, only the 'large' ones seem to break down, while for $n > 1$ *every solution* ultimately develops a discontinuity. This is consistent with our TW analysis.
- We briefly consider an alternative saturation mechanism with $Q = Q(u_x/u)$. In this case, the competition between the nonlinear convection and diffusion becomes even more interesting: a compactly supported solution may now develop discontinuities *at both ends of the support,* with the left discontinuity propagating in the opposite direction to the motion induced by the convection.

This paper is organized as follows. In the next section, we compute TW solutions and describe how discontinuities emerge if TWs are to exist. In section 3, we show that 'small' amplitude solutions are classical solutions, while in section 4, the breakdown of 'large' amplitude semi-compactly supported solutions is proved. Evolution of compactly supported initial data for equation (1.1) is numerically studied in section 4.1. The impact of the alternative saturation mechanism with $Q = (\ln u)_x$ is studied in section 4.2. Finally, in appendix A we exemplify the effects of saturated diffusion on a plane. In appendix B we describe the numerical approach used to study our problem.

2. Travelling waves

In this section, we study the behaviour of TW solutions of (1.1) that satisfy

$$U(z) = u(x - \lambda t), \qquad U(-\infty) = U_L > 0, \quad U(\infty) = 0. \tag{2.1}$$

Substituting (2.1) into (1.1) results in the ODE

$$-\lambda U' + [f(U)]' = [\varphi(U)Q(U')]',$$

which can be integrated to obtain

$$Q(U') = \frac{f(U)U_L - f(U_L)U}{\varphi(U)U_L}, \qquad \lambda = \frac{f(U_L)}{U_L}. \tag{2.2}$$

It is now clear that if the right-hand side (RHS) of (2.2) is out of the domain of Q for some $U \in [0, U_L]$, then the solution of (2.2) cannot be continuous.

Further analysis of (2.2) can be carried out in every concrete case. A typical example is as follows.

Example. $f(u) = u^2$, $\varphi(u) = u^n$ and Q given by (1.3):

$$u_t + (u^2)_x = [u^n Q(u_x)]_x. \tag{2.3}$$

Now equation (2.2) reads

$$Q(U') = U^{1-n}(U - U_L), \qquad \lambda = U_L, \tag{2.4}$$

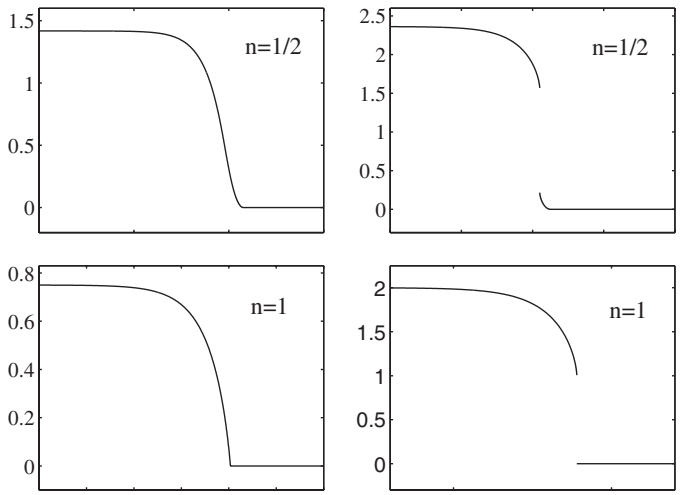

Figure 1. TW solutions of (2.3) for subcritical $U_L = 0.75U^*$ (left column) and supercritical $U_L = 2U^*$ (right column).

and its solution will be continuous only if the RHS of (2.4) belongs to the domain of Q, i.e. if

$$-1 \leqslant U^{1-n}(U - U_L) \leqslant 1, \qquad \forall U \in [0, U_L], \tag{2.5}$$

which merely specifies the domain where inertial and viscous forces balance each other. Depending on the values of n, there are several cases to be considered (the $n = 0$ case was studied in [11]).

Case I. If $0 < n < 1$, one easily checks that the inequality (2.5) holds if and only if

$$U_L \leqslant U^* := \frac{2-n}{(1-n)^{(1-n)/(2-n)}},$$

where U^* is the critical value, for which the solution is still continuous, but has an infinite gradient at one point. If $U_L > U^*$, then no continuous solution is possible, and the resulting (weak) solution contains a subshock with the left- and right-sided values that can be obtained from the equation

$$U^{1-n}(U - U_L) = -1. \tag{2.6}$$

Note that both the left- and the right-sided limits of U' at the subshock are equal to $-\infty$.

In figure 1, we show both smooth and discontinuous TWs, obtained in the sub- and supercritical cases, respectively.

Case II. For $n = 1$, equation (2.4) reduces to

$$Q(U') = U - U_L,$$

and it immediately follows that the critical value of U_L is $U^* = 1$ (see figure 1). Also note that in the supercritical case, the size of the jump is equal to $U_L - 1$.

Case III. Finally, if $n > 1$, the RHS of (2.4) is always smaller than -1 for $U \sim 0$, and therefore its solution must contain a subshock. A typical TW solution is similar to the supercritical TW in case II.

Remarks.

1. In cases II and III, the left-side limit of U' at the subshock is equal to $-\infty$ (as in case I), while the right-sided limit is 0.

2. In the supercritical cases, the speed of subshocks can also be computed from the Rankine–Hugoniot condition:

$$s = \frac{[u^2 - u^n Q(u_x)]}{[u]}. \tag{2.7}$$

In cases II and III, where the right-sided subshock value is equal to zero, (2.7) reduces to

$$s = \frac{U_-^2 - U_-^n Q(U'_-)}{U_-} = U_- + U_-^{n-1}, \tag{2.8}$$

where U_- denotes the left-sided value on the subshock.

Note that for TWs, s must be equal to λ, which implies that equation (2.8) is, in fact, equivalent to (2.6).

3. In a more general case, when $f(u) \sim u^m$, $m > 1$, $\varphi(u) \sim u^n$ for $u \sim 0$, the conclusions of the TW analysis are similar, though the critical values of U^* will be different.
4. Our TW study shows that equation (1.1) admits both smooth and discontinuous solutions. The latter ones are weak solutions that satisfy definition 1 in [19]. In the next section, we demonstrate numerically that both smooth and discontinuous TW solutions may emerge out of a wide class of initial data; i.e. they are strong attractors.

2.1. Stability of travelling waves

We begin with the proof of their L^1-stability. Let $\omega_0(x)$ be a (small) perturbation added to the TW. The solution of (1.1) is then sought in the form $u(x,t) = U(x - \lambda t) + \omega(x,t)$, $\omega(x,0) := \omega_0(x)$, which results in

$$U_t + \omega_t + f(U+\omega)_x = [\varphi(U+\omega) \cdot Q(U' + \omega_x)]_x.$$

Using the Taylor expansion yields

$$\omega_t + [\omega f'(\tilde{U})]_x = [\omega_x \varphi(U) Q'(\hat{U}') + \omega \varphi'(\bar{U}) Q(U')]_x,$$

where $\tilde{U}$, $\hat{U}$, $\bar{U}$ are the corresponding intermediate values. Finally, we multiply the last equation by $\operatorname{sgn}(\omega)$ and integrate over x. Then, the positivity of φ and Q' implies that for all t

$$\frac{\mathrm{d}}{\mathrm{d}t}\|\omega\|_{L^1} \leqslant 0. \tag{2.9}$$

Note that the above calculation only shows that a perturbation does not increase in time, but does not guarantee that $\omega \to 0$ in the L^1-norm. Even though we cannot *yet prove the latter*, our numerical experiments clearly indicate that (even large) perturbations decay rapidly, and hence the TW solutions are strong attractors. In figures 2 and 3, we show numerical solutions of (2.3) with $n = 1/2$ and $n = 1$, respectively, as well as the exact solution obtained by solving equation (2.4). The solutions are computed for 'small' and 'large' U_L, and smooth or discontinuous initial data. The convergence appears to be very good: one can hardly notice the difference between the numerical and the exact solution. Note that in figures 2 and 3(*a*) the numerical and exact solutions are plotted at $t = 4$, while in figure 3(*b*) the solutions are presented at time $t = 8$, since in this case the convergence is much slower.

3. Classical solutions for a 'small' initial datum

As observed in the previous section, equation (1.1) admits both classical, smooth and weak, discontinuous solutions. A notion of a weak solution for models with saturating dissipation was

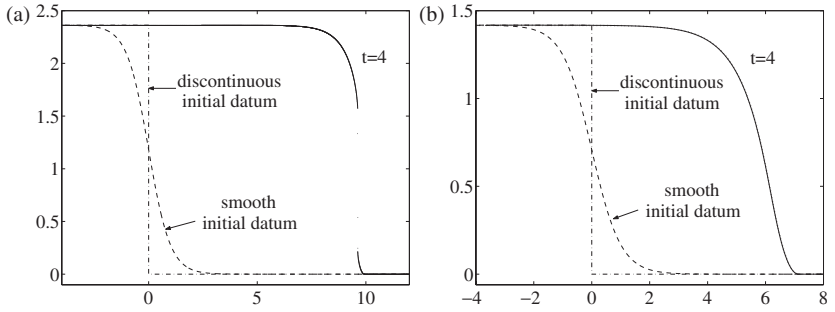

Figure 2. Solution of (2.3) with $n = 1/2$ and smooth and discontinuous initial data for (a) 'large' $U_L = 1.25U^*$ and (b) 'small' $U_L = 0.75U^*$. The computed solutions ($\cdots\cdots$) at time $t = 4$ almost coincide with the asymptotic TW solution (——).

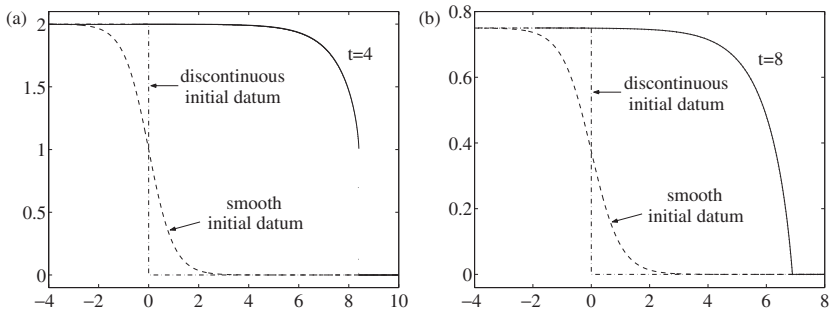

Figure 3. Solution of (2.3) with $n = 1$ and smooth and discontinuous initial data for (a) 'large' $U_L = 2U^*$ and (b) 'small' $U_L = 0.75U^*$. The computed solutions ($\cdots\cdots$) almost coincide with the asymptotic TW solution (——).

given in [5, 19], see also [11]. Existence and uniqueness of the weak solution of equation (1.1) is still an open problem. However, in the case of 'small' positive smooth initial data, the solution will retain its initial smoothness. The proof follows the arguments presented in [11], and is based on the uniform boundedness of u_x, shown in the following lemma.

Lemma 3.1. *Let $u(x, t)$ be a classical positive solution of the IVP (1.1)–(1.2), and let $Q : \mathbb{R} \to (a, b)$, where $a < 0$ and $b > 0$. If the smooth initial datum is bounded away from zero,*

$$0 < m := \min_x u_0(x) \leqslant u_0(x) \leqslant \max_x u_0(x) =: M, \qquad \forall x \tag{3.1}$$

and satisfies the following assumption,

$$\frac{\varphi(M)}{\varphi(m)} \| Q(u_0') \|_{L^\infty} + 2 \| f(u_0) \|_{L^\infty} \leqslant \alpha < \min(-a, b), \tag{3.2}$$

then for all $t \geqslant 0$

$$\| u_x \|_{L^\infty} \leqslant C.$$

Proof. First, we note that the solution of the (degenerate) parabolic equation (1.1) satisfies a maximum principle, which guarantees that

$$m \leqslant u(x, t) \leqslant M, \qquad \forall x, \forall t \geqslant 0. \tag{3.3}$$

We then rewrite equation (1.1) as

$$u_t = z_x, \tag{3.4}$$

where

$$z := \varphi(u)Q(u_x) - f(u). \tag{3.5}$$

Differentiating (3.5) with respect to t and using (3.4), we obtain

$$z_t = [\varphi'(u)Q(u_x) - f'(u)]z_x + \varphi(u)Q'(u_x)z_{xx}. \tag{3.6}$$

Since $\varphi(u) \geqslant \varphi(m) > 0$ for $u \geqslant m$ and $Q'(s) > 0$ for all s, equation (3.6) remains parabolic $\forall t > 0$, and its solution satisfies a maximum principle:

$$|\varphi(u)Q(u_x) - f(u)| \leqslant |\varphi(u_0)Q(u_0') - f(u_0)|, \qquad \forall t \geqslant 0. \tag{3.7}$$

Finally, using the triangle inequality, (3.2) and (3.3), we obtain

$$|Q(u_x)| \leqslant \alpha, \qquad \forall t \geqslant 0.$$

The monotonicity of Q and the last inequality imply that there exists a constant C such that $|u_x| \leqslant C$. This completes the proof of the lemma. ■

Utilizing lemma 3.1 and following similar arguments to those found in [11] one obtains existence and uniqueness results (the proof is omitted).

Theorem 3.1 (existence and uniqueness of classical solutions). *Consider the IVP (1.1)–(1.2). Assume that the initial datum $u_0(x) \in C^3$ satisfies the assumptions (3.1) and (3.2). Then there exists a unique global classical solution of (1.1)–(1.2), $u(x, t) \in C^{2,1}(x, t)$.*

4. Breakdown of 'large' initial datum

We now use the special case $\varphi(u) = u$, to demonstrate that the solution of (1.1)–(1.2) may break down within a finite time even if it is infinitely smooth within the semi-compact support.

Our proof follows the comparison technique presented in [8]. However, the breakdown of solutions of equation (1.1) with $\varphi(u) \equiv 1$ shown in [8], relies on the use of skew symmetric initial data and thus cannot be extended 'as is' to the present situation wherein the solutions studied are non-negative. We also call the reader's attention to our earlier work [7], where it was shown that in the absence of convection a compactly supported non-negative solution of equation (1.4) with $n > 1$ breaks down within finite time, either within its support or at the front(s). Obviously, the presence of convection will not change the situation. The only notable change may occur for $n \leqslant 1$. For instance, for $n = 1$ without convection there is no breakdown; however, the combination of nonlinear convection and saturated diffusion flux,

$$u_t + f(u)_x = [uQ(u_x)]_x, \tag{4.1}$$

may cause 'large' solutions to develop discontinuities.

Throughout this section we assume that the flux functions, f and Q, satisfy the following conditions:

(i) Q is a strictly monotone ($Q'(s) > 0\,\forall s$), skew symmetric ($Q(-s) = -Q(s)\,\forall s$), bounded function, satisfying $Q(s) \to Q_\infty < \infty$ as $s \to \infty$;

(ii) f is a strictly monotone ($f'(u) > 0\,\forall u > 0$), convex ($f''(u) > 0\,\forall u > 0$) function, satisfying $f(u) \sim u^\alpha$, $\alpha > 1$ for $u \sim 0$ and $\lim_{u\to\infty}(f(u)/u) = \infty$.

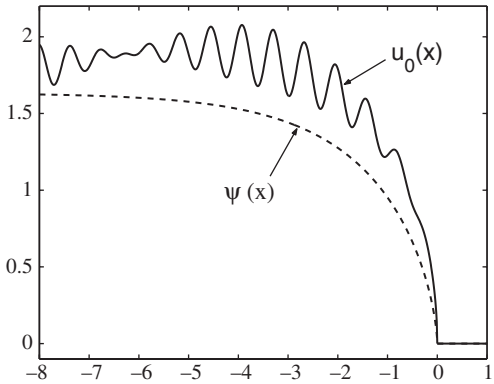

Figure 4. A function $\psi(x)$ and an initial datum $u_0(x)$ satisfying hypotheses (a) and (b).

We also assume that a continuous initial datum satisfies the following hypotheses (a typical initial datum is shown in figure 4):

(a) $u_0(x)$ is a smooth positive function on a semi-infinite interval $(-\infty, x_f(0))$, while $u_0(x) \equiv 0$ for $x \geqslant x_f(0)$ (we denote by $x_f(t)$ the location of the front at time t);
(b) $u_0(x) \geqslant \psi(x)\, \forall x < x_f(0)$.

Here ψ is a semi-compact profile to be determined. In what follows we will, without loss of generality, assume that $Q_\infty = 1$ and $x_f(0) = 0$.

Let us first make the following change of variables,

$$z = x - t, \qquad \tau = t, \tag{4.2}$$

and rewrite equation (4.1) in the new variables (renaming again $t := \tau$):

$$u_t + (f(u) - u)_z = [u\,Q(u_z)]_z. \tag{4.3}$$

Next, we consider the following auxiliary boundary-value problem (BVP):

$$-B(\psi)_z + f(\psi)_z = m[\psi\, Q(\psi_z)]_z, \tag{4.4}$$

$$\psi(0) = 0, \qquad \psi(-\infty) = \bar{u}, \tag{4.5}$$

where the function B is continuous on $[0, \bar{u}]$, $B(u) \sim u$ for $u \sim 0$, and $B(\bar{u}) = f(\bar{u})$. Integrating (4.4) and taking into account the boundary conditions (4.5), we obtain

$$-B(\psi) + f(\psi) = m\psi\, Q(\psi_z),$$

thus,

$$Q(\psi_z) = \frac{f(\psi) - B(\psi)}{m\psi}. \tag{4.6}$$

Since B and f are continuous bounded functions and since the limit of the RHS of (4.6) as $\psi \to 0$ is finite, it is clear that for sufficiently large positive m, equation (4.6) has a unique solution, which also solves the BVP (4.4)–(4.5). Note that condition (ii) implies that at the front, where $\psi = 0$, $Q(\psi_z) = -1$, and thus the (left-sided) derivative ψ_z is equal to $-\infty$ there (see figure 4).

We now demonstrate that for an appropriate choice of $\bar{u}$ and B, the solution of (4.4)–(4.5) exists for any m and is a subsolution to equation (4.3). To prove the latter, we need to show that

$$(f(\psi) - \psi)_z \leqslant [\psi\, Q(\psi_z)]_z. \tag{4.7}$$

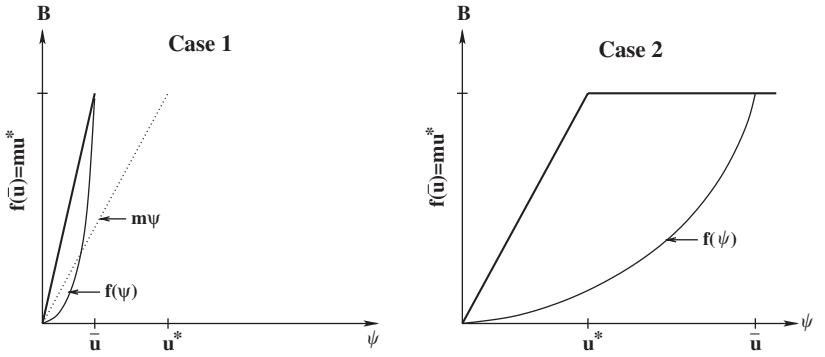

Figure 5. The function $B(\psi)$ given by (4.10).

Multiplying (4.7) by m and subtracting from it equation (4.4) we obtain

$$\{[B'(\psi) - m] + (m-1)f'(\psi)\}\psi_z \leqslant 0. \tag{4.8}$$

The inequality (4.8) will be satisfied if we take the function B, constructed as follows. Let $m > 1$ be a (large) number and let u^* be a positive number such that

$$f'(u^*) = \frac{m}{m-1}. \tag{4.9}$$

Then, we take $\bar{u} > 0$ that satisfy $f(\bar{u}) = mu^*$ and

$$\begin{aligned} &B(\psi) = \frac{f(\bar{u})}{\bar{u}}\psi, \qquad \text{if } \bar{u} \leqslant u^* \text{ (case 1)},\\ &B(\psi) = \begin{cases} m\psi, & \text{for } 0 \leqslant \psi \leqslant u^*,\\ f(\bar{u}), & \text{for } u^* < \psi \leqslant \bar{u}, \end{cases} \qquad \text{if } \bar{u} > u^* \text{ (case 2)}, \end{aligned} \tag{4.10}$$

see figure 5.

It is now clear that for this B the RHS of (4.6) is between -1 and 0, and thus there exists a unique continuous solution of (4.4)–(4.5), ψ, used in hypothesis (b). In order to verify the inequality (4.8), we first note that since $B(\psi) \geqslant f(\psi)$ for all $\psi \in [0, \bar{u}]$, equation (4.6) implies $\psi_z \leqslant 0$. The second term on the left-hand side of (4.8), $[B'(\psi) - m] + (m-1)f'(\psi)$, is non-negative since $m > 1$ and due to our choice of B, (4.10), and the convexity of f.

We are now ready to prove our main result concerning the breakdown of equation (4.1).

Theorem 4.1 (breakdown of semi-compactly supported solutions). *Consider equation (4.1) subject to a semi-compactly supported, smooth, non-negative initial datum (1.2). Let hypotheses (i)–(ii) and (a)–(b) be satisfied. Suppose that $u(x,t)$ is a semi-compactly supported weak solution of (4.1) and (1.2), which remains continuous on the interval $(-\infty, x_f(t))$, for all $t \geqslant 0$. Then there exists a finite time bound $T^* > 0$, such that no later than at $t \leqslant T^*$, $u(x,t)$ has a jump discontinuity at $x = x_f(t)$.*

Proof. We first make a change of variables (4.2), which allows us to study equation (4.3) rather then the original equation (4.1). Let us now assume that the solution of (4.3), (1.2), $u(z,t)$, remains continuous for all $t \geqslant 0$; then its front does not move, i.e. $z_f(t) \equiv z_f(0) = 0$. Indeed, at the front $u(z_f(t), t) = 0$, and thus the speed of the front, $\dot{z}_f(t)$, which is determined via $f'(u) - 1 - Q(u_z)$, vanishes at $(z_f(t), t)$, because $Q(u_z) = -1$ there. Note that the latter is true due to hypothesis (b), the unboundedness of ψ_z at the front, and the comparison principle.

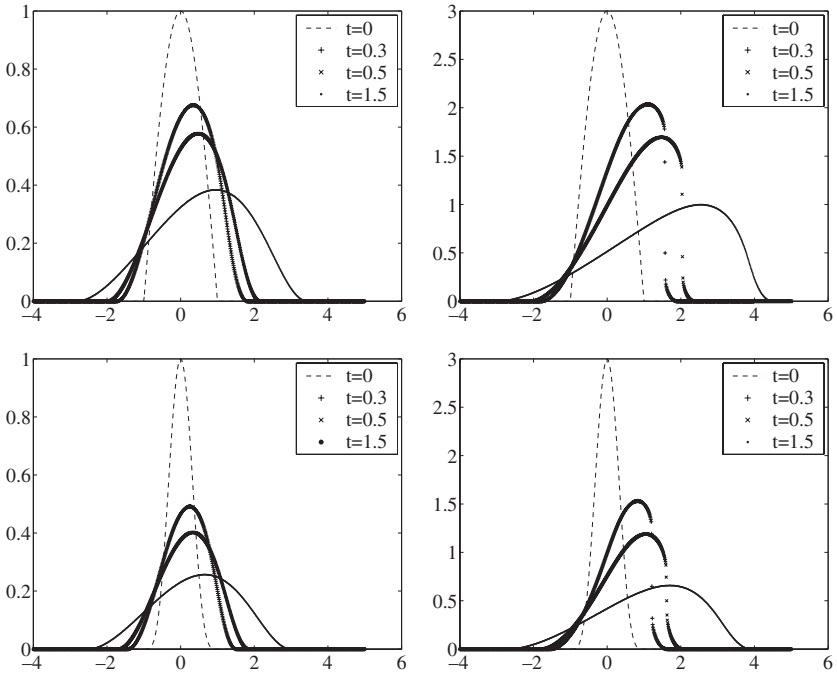

Figure 6. Solution of (2.3), (4.12) (upper row) and (2.3), (4.13) (lower row) with $n = 1/2$ for 'small' $A = 1$ and 'large' $A = 3$ initial datum.

Next, let $a > 0$ be a sufficiently large number and integrate equation (4.3) with respect to z:

$$\frac{\mathrm{d}}{\mathrm{d}t}\int_{-a}^{0} u(z,t)\,\mathrm{d}z = f(u(-a,t)) - u(-a,t)[1 + Q(u_z(-a,t))]. \tag{4.11}$$

Using hypotheses (ii) and (b) and the comparison principle, the RHS of (4.11) can be bounded from below by the positive constant $\gamma := \frac{1}{2}(f(\bar{u}) - 2\bar{u})$ provided a and $\bar{u}$ are sufficiently large (note that $\bar{u}$, determined via $f(\bar{u}) = mu^*$, can be made adequately large by taking m large, since, as it follows from (4.9), u^* is bounded away from zero). Therefore, there exists a finite time T^* such that

$$\int_{-a}^{0} u(z,T^*)\,\mathrm{d}z = a\|u_0\|_{L^\infty},$$

which cannot be satisfied by a continuous function u. This contradiction implies that the solution must develop a jump discontinuity at the front at some time $t \leqslant T^*$, which, in turn, induces the motion of the front (or, in terms of the original coordinates of equation (4.1), will accelerate the front), which invalidates (4.11). ■

4.1. Breakdown of a compactly supported initial datum

We now present numerical studies of equation (2.3) subject to continuous compactly supported initial data:

$$u_0(x) = \begin{cases} A\cos\left(\dfrac{\pi x}{2}\right), & \text{if } x \in [-1,1], \\ 0, & \text{otherwise,} \end{cases} \tag{4.12}$$

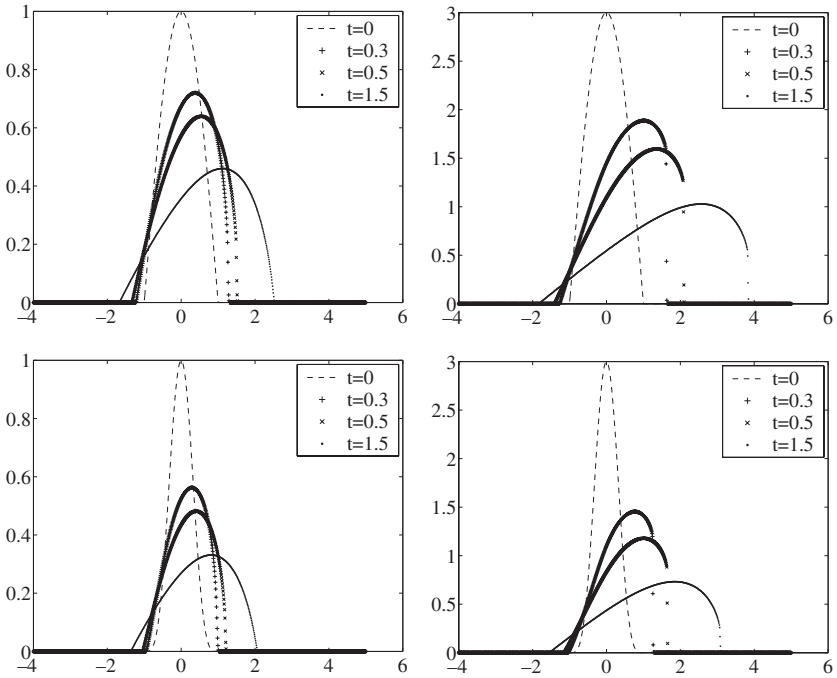

Figure 7. Solution of (2.3), (4.12) (upper row) and (2.3), (4.13) (lower row) with $n = 1$ for 'small' $A = 1$ and 'large' $A = 3$ initial datum.

and

$$u_0(x) = \begin{cases} A\cos^4\left(\dfrac{\pi x}{2}\right), & \text{if } x \in [-1, 1], \\ 0, & \text{otherwise.} \end{cases} \tag{4.13}$$

In figures 6–8 we show the numerical solution of (2.3), (4.12) and (2.3), (4.13) with $n = 1/2$, $n = 1$, and $n = 2$ respectively, for 'small' ($A = 1$) and 'large' ($A = 3$) initial data. As one can see, in the $n = 1/2$ and $n = 1$ cases, though the profiles of the pulses change, the solution remains continuous for 'small' initial data. However, for 'large' initial data the evolving solution goes through two phases. Take, for instance, the $n = 1/2$ case; in the beginning, the initially large profile develops sharp discontinuities, which later, however, completely disappear. In the $n = 1$ case, one observes a similar effect but it takes longer for discontinuities to resolve. The difference is shown in figure 9 (snapshots of the solution of (2.3), (4.12) with $n = 1$ and $A = 3$ at $t = 1.5, 2.5, 3.5$). In both cases, though initial conditions enforce the discontinuity on the system, it cannot be sustained for long. On the other hand, in the $n = 2$ case, the solution breaks down even for 'small' initial data, and remains discontinuous thereafter.

It is also instructive to demonstrate the qualitative differences between the cases of linear and saturated fluxes for the $n > 1$ cases, with and without convection. In figures 10–13 we follow the evolution of the same initial pulse (4.13) for different problems. In figure 14 the long time asymptotic behaviour of the solutions of equation (2.3) with linear and saturated fluxes as well as that of the solution of the corresponding inviscid equation (with $Q \equiv 0$) are shown. Note that in the inviscid case, the front has a higher velocity. Absence of dissipation is also reflected in the fact that the sharp discontinuous front has a larger amplitude. If the

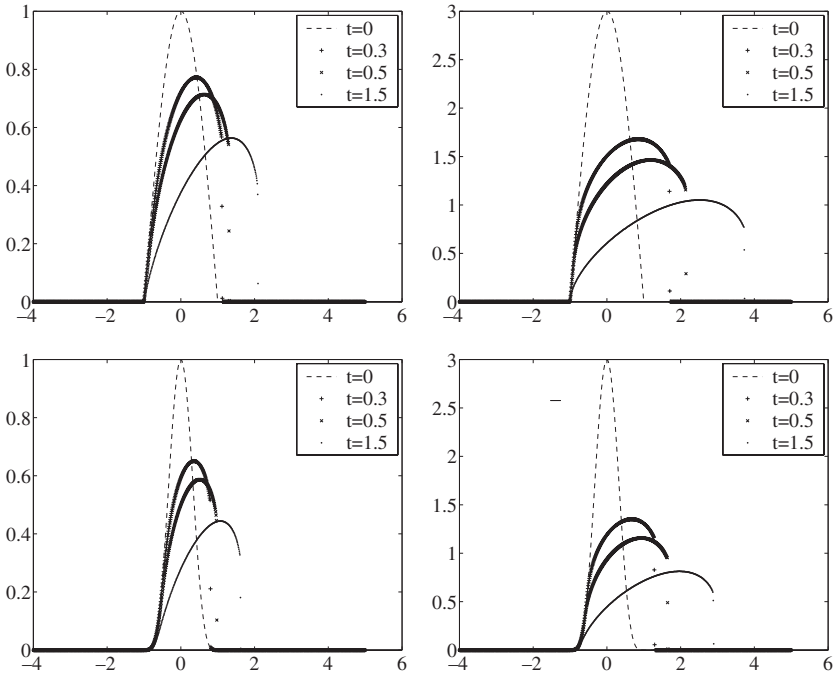

Figure 8. Solution of (2.3), (4.12) (upper row) and (2.3), (4.13) (lower row) with $n = 2$ for 'small' $A = 1$ and 'large' $A = 3$ initial datum.

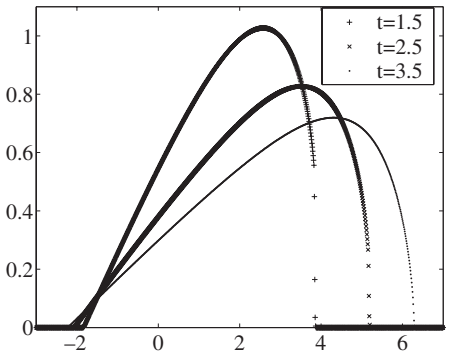

Figure 9. Solution of (2.3), (4.12) with $n = 1$ and 'large', $A = 3$, initial data at $t = 1.5, 2.5, 3.5$. Note that the discontinuity at $t = 1.5$ has completely disappeared at $t = 3.5$.

diffusion coefficient (assumed in all cases to be equal to one) is made smaller the distinction between the inviscid and dissipative cases diminishes.

The examples presented also clearly exhibit the impact of saturated diffusion on the time at which the front starts to move. This so-called waiting time effect was studied in some detail without convection, which, as expected and clearly seen in the displayed examples, hastens the formation of discontinuity at the right (left) front for $f'(u) > 0$ ($f'(u) < 0$), and thus shortens the waiting time. Interestingly, the long time behaviour shows that the attended profiles in the cases of the linear and saturating diffusion fluxes, apart from the differences across the front layer, are almost identical. In the layer, the solution of (2.3) with nonlinear Q seems to be

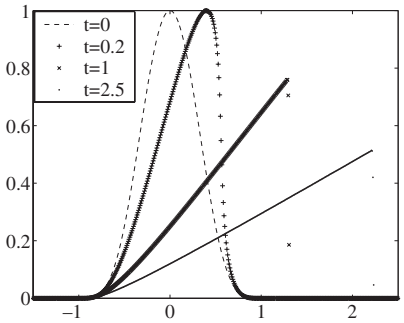

Figure 10. Solution of $u_t + (u^2)_x = 0$ subject to the initial datum (4.13) with $A = 1$.

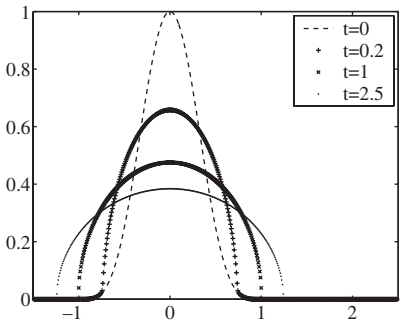

Figure 11. Solution of $u_t = (u^2 u_x)_x$ subject to the initial datum (4.13) with $A = 1$. Note the delay in the motion of the fronts. This effect, as shown in the next figure, is further enhanced if the saturation mechanism is turned on.

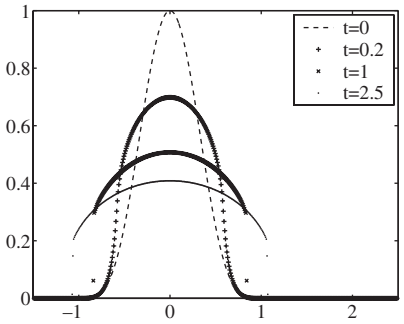

Figure 12. Effects of a saturated diffusion: solution of (1.4), (4.13) with $n = 2$ and $A = 1$. Note the delayed propagation of the fronts which do not move until a sharp discontinuity forms.

discontinuous while, as is well known, the solution of this equation with linear Q is continuous but has an infinite gradient at the front.

4.2. An alternative saturation mechanism

In this section, we study the equation

$$u_t + f(u)_x = \left[u^n Q\left(\frac{u_x}{u}\right)\right]_x, \tag{4.14}$$

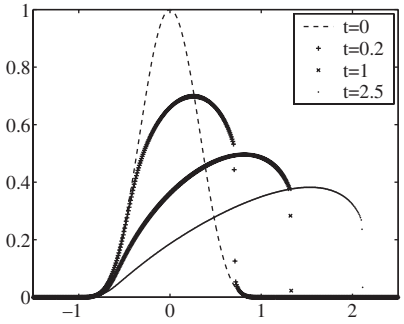

Figure 13. Solution of (2.3), (4.13) with $n = 2$ and $A = 1$. Adding convection to a saturated diffusion, hastens the formation of a discontinuous front and thus its motion. (Compare with the previous figure at, say $t = 0.2$.)

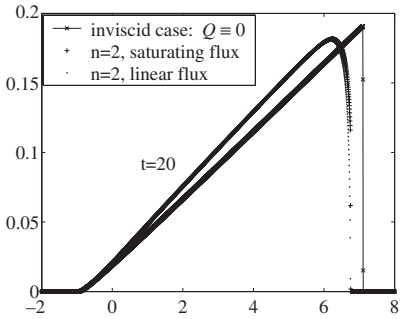

Figure 14. Solutions of (2.3), (4.13) with $n = 2$ and $A = 1$, after a long time. The evolution of the same initial datum, but either with linear Q or without diffusion ($Q \equiv 0$) is also shown. Note the impact that the diffusion has on the slope and on the front speed in the various cases.

for which the competition between the nonlinear convection and the saturating diffusion may become even more interesting. TW solutions of (4.14) are similar to those discussed in section 2, and thus we concentrate on compactly supported solutions and rarefaction-type waves. We consider a particular case, in which $f(u) = u^m$, Q given by (1.3), and thus equation (4.14) reduces to

$$u_t + (u^m)_x = \left[\frac{u^n u_x}{\sqrt{u^2 + u_x^2}} \right]_x . \tag{4.15}$$

We first numerically solve equation (4.15) with $m = 2$ and different values of n, subject to compactly supported initial data (4.12). One can observe from figure 15(a) that the solution breaks down at both ends of its support, and then the fronts propagate in the opposite directions. This illustrates that when $n = 3/2$, the behaviour of the left front is dominated by the saturated diffusion, while the right front is dominated by nonlinear convection, and only its shape is affected by the presence of the nonlinear diffusion. In figure 15(b), $m = n = 2$. Note that the outcome of the competition between convection and diffusion is now different: *the left front does not seem to move at all.* In the third case ($n = 3$), both fronts are dominated by the convection (see figure 15(c)).

Remark. In general, our numerical experiments (not shown here) demonstrate that the solutions in the $m > n > 1$ domain are similar to the solution in figure 15(a), while the

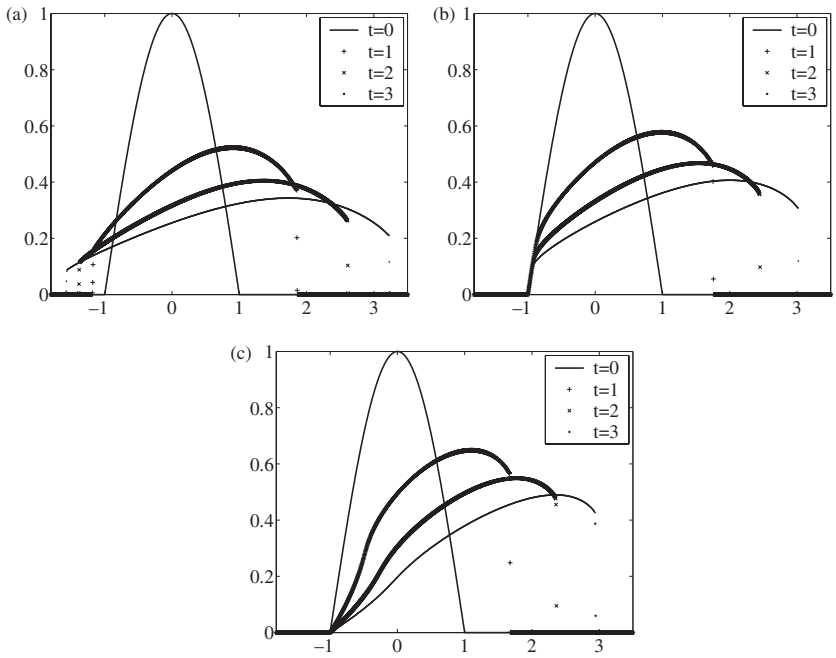

Figure 15. Solutions of (4.15), (4.12) with $m = 2$; (*a*) $n = 3/2$, (*b*) $n = 2$ and (*c*) $n = 3$.

$m = n > 1$ and $n > m > 1$ domains are represented well by figures 15(*b*) and 15(*c*), respectively.

Next, we consider equation (4.15) with $m = 2$ and $n = 3/2$ subject to the following smooth initial data:

$$u_0(x) = A(1 + \tanh(Kx)), \qquad A > 0, \quad K > 0. \tag{4.16}$$

It is obvious that in the purely convective case (no diffusion) such a datum will evolve into continuous rarefaction waves. However, in the presence of the saturated diffusion we may obtain a break down! Even though a rigorous breakdown criterion is not available, we can easily demonstrate numerically that if an initial gradient is 'large', the solution develops a left-moving discontinuity (see figure 16(*a*)), while the solution with 'small' initial gradients remains smooth (see figure 16(*b*)).

5. Summary

In weakly nonlinear models, with the Burgers equation being the most relevant example, competing mechanisms (here inertia versus dissipation) remain in a detailed balance at all amplitudes. This feature which is typical of all model equations derived under the weakly nonlinear assumption, rarely holds in actual physical set-ups. When equations derived under the assumption of small amplitudes and gradients, are then employed in the fully nonlinear regime, their predictions are then an accidental byproduct of the weakly nonlinear regime. The model presented in this work aims to model a genuinely nonlinear scenario wherein the balance between two specific competing mechanisms may break down due to the inability of one of the competing forces (the dissipation) to counteract the other (inertia). Within the frame of the given model the emerging shock is a resolution of structural frustration. In a

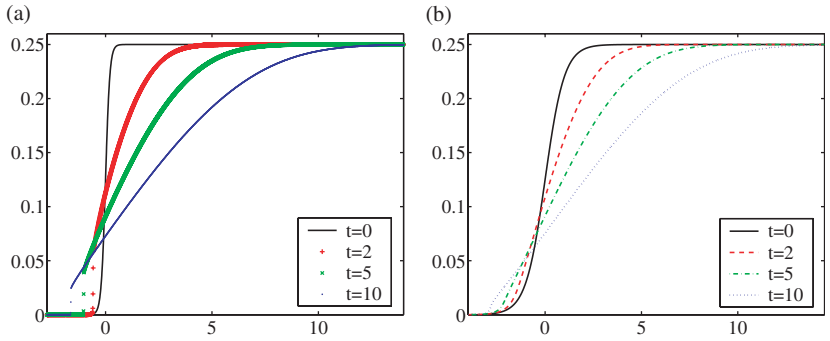

Figure 16. Solutions of (4.15)–(4.16) with $m = 2$, $n = 3/2$, $A = 0.125$; (*a*) $K = 5$ and (*b*) $K = 1$.

wider, scientific, context the shock represents a collapse of a boundary layer calling for the intervention of other, neglected, mechanisms.

Acknowledgments

The research of AK was supported in part by the NSF grants # DMS-0196439 and # DMS-0310585. The work of AC was supported in part by the NSF grant # DMS-0410023.

Appendix A. Saturated diffusion on a plane

We present a brief summary of saturated diffusion in a plane. The equation to be studied is a two-dimensional extension of equation (1.4):

$$u_t = [u^n Q(u_x, u_y)]_x + [u^k R(u_x, u_y)]_y, \qquad n > 0, \quad k > 0, \tag{A.1}$$

where Q and R are smooth bounded functions, satisfying the condition of (weak) parabolicity (see, e.g. [13]). Typical diffusion fluxes that have been used in our numerical experiments are

$$Q(u_x, u_y) = \left(\frac{u_x}{\sqrt{1 + u_x^2 + u_y^2}} \right)_x, \qquad R(u_x, u_y) = \left(\frac{u_y}{\sqrt{1 + u_x^2 + u_y^2}} \right)_y. \tag{A.2}$$

In the examples presented, we use (A.1)–(A.2) with $n = k = 3$ and the following data.

Example 1.

$$u(x, y, 0) = \begin{cases} \cos\left(\frac{\pi x}{2}\right) \cos^4\left(\frac{\pi y}{2}\right), & \text{if } (x, y) \in [-1, 1] \times [-1, 1], \\ 0, & \text{otherwise.} \end{cases} \tag{A.3}$$

The numerical solutions of the IVP (A.1)–(A.3) shown in figures A1–A3 describe the evolution at $t = 0, 1, 3, 5, 20$ and 150.

The simulation presented demonstrates three effects.

1. Formation of discontinuities prior to initiation of fronts motion.
2. The waiting time phenomenon, which imposes a different delay on different parts of the front and thus may initially cause an isotropic propagation of the front (compare the location of the front in different planar projections).
3. Convergence towards universal patterns at large times.

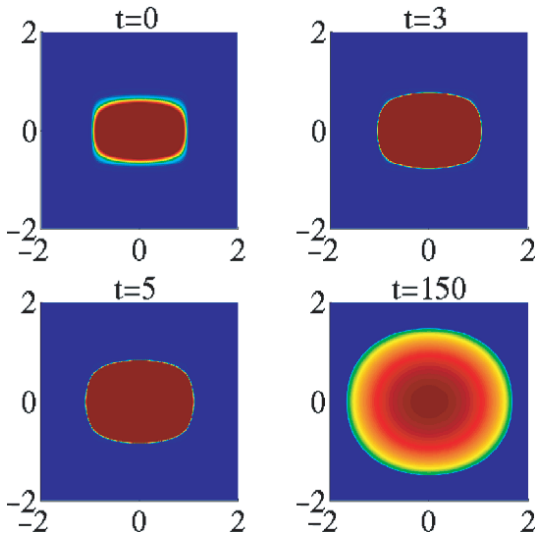

Figure A1. Solution of (A.1)–(A.3) with $k = n = 3$: top view.

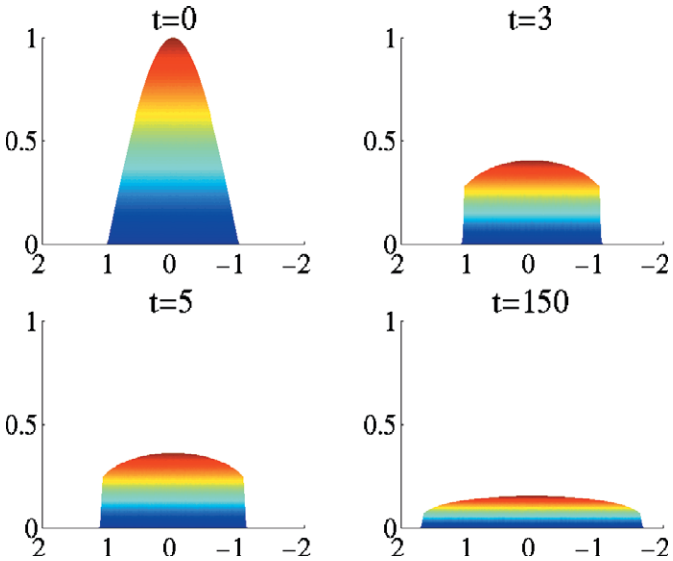

Figure A2. Solution of (A.1)–(A.3) with $k = n = 3$: projection onto the (x, z)-plane.

Example 2.

$$u(x, y, 0) = \begin{cases} \cos^{\alpha}\left(\dfrac{\pi r}{2}\right), & \text{if } r := \sqrt{x^2 + y^2} > 1, \\ 0, & \text{otherwise,} \end{cases} \tag{A.4}$$

where

$$\alpha = \frac{1}{2}\left[3\tanh\left(5\theta - \frac{5\pi}{4}\right) + 5\right],$$

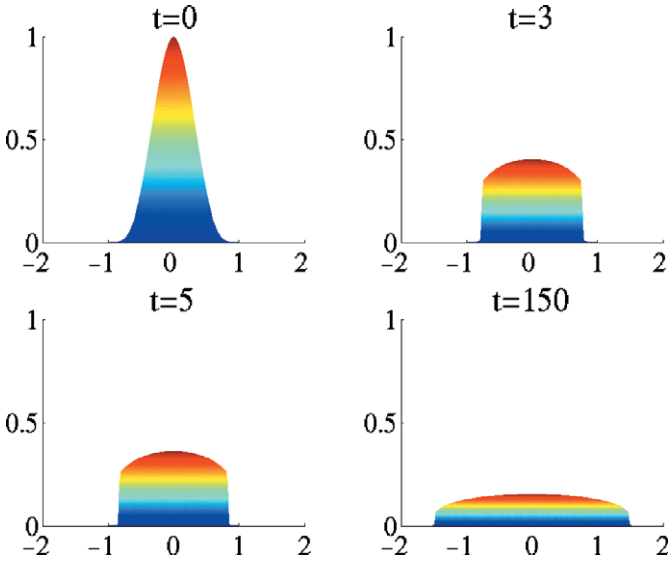

Figure A3. Solution of (A.1)–(A.3) with $k = n = 3$: projection onto the (y, z)-plane. Note the location of the support at various times.

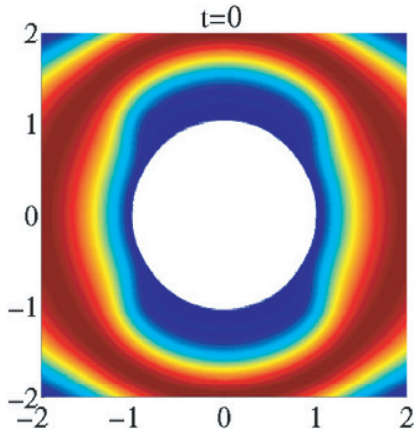

Figure A4. The initial data in example 2.

and

$$\theta = \begin{cases} \arctan\left|\dfrac{y}{x}\right|, & \text{if } x \neq 0, \\ 0, & \text{if } x = 0. \end{cases}$$

The initial datum is shown in figure A4. The computational domain is the square $[-2, 2] \times [-2, 2]$ with the Neumann boundary conditions:

$$u_x(-2, y, t) = u_x(2, y, t) = u_y(x, -2, t) = u_y(x, 2, t) = 0. \tag{A.5}$$

The numerical solutions of the initial-boundary value problem (IBVP) (A.1)–(A.2), (A.4)–(A.5) at times $t = 10$, 20 and 30 are presented in figures A5 and A6. For comparison purposes, in figure A7, we show the solution of the same IBVP but with the linear diffusion fluxes $Q(u_x, u_y) = u_x$ and $R(u_x, u_y) = u_y$.

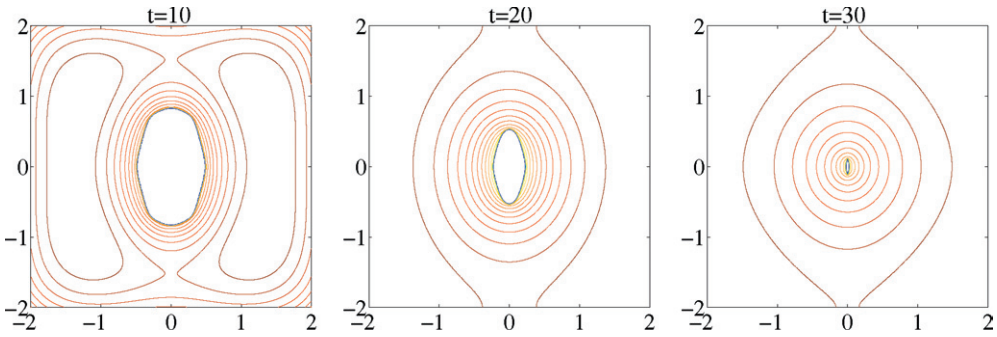

Figure A5. Solutions of the IBVP (A.1)–(A.2), (A.4)–(A.5) with $k = n = 3$ at different times.

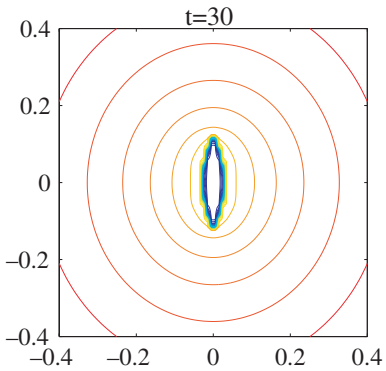

Figure A6. Solution of the IBVP (A.1)–(A.2), (A.4)–(A.5) with $k = n = 3$ at time $t = 30$—zoom at the centre of the domain.

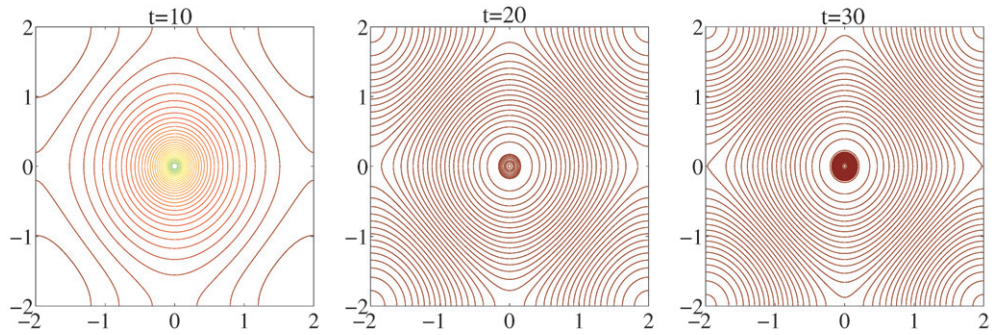

Figure A7. Solutions of the IBVP (A.1)–(A.2), (A.4)–(A.5) with $k = n = 3$ and linear Q and R at different times.

To see the dramatic effect of anisotropy induced by initial data and preserved due to the saturation of diffusion, one is advised to look first at the 'classical' nonlinear diffusion in figure A7: at $t = 10$ the initial hole has essentially disappeared, and at $t = 20$ and thereafter, a steady state has been practically attained. In contrast with the classical case, when the diffusion flux saturates, the presence of initial anisotropy slows the diffusion and causes a different rate of diffusion in different directions. Unlike an external problem, like the one

considered in example 1, the finiteness of the domain does not provide enough time for a 'diffusive catch up' which ultimately renders the process isotropic. The net effect is that the initial hole closes towards a one-dimensional slit. This is evident from the displayed graphs. Indeed, if one normalizes the width of the hole in the y-direction, say, to one, the width in the x-direction shrinks in the ratio of about $1.8 : 1.3 : 0.8$, at $t = 10, 20, 30$, respectively. In those normalized units the compression in the x-direction propagates approximately at a constant rate, though numerical accuracy prevents us from making a more detailed analysis of this fascinating phenomenon.

Appendix B. Numerical methods

As it has been demonstrated in the numerical examples, presented in section 4, the discontinuities developed in the models studied are due to two (competing) mechanisms: nonlinear convection and saturated diffusion. These discontinuities may emerge from smooth initial data, then they propagate and their amplitudes typically decrease in time, and in some cases the developed discontinuities may even disappear at later times (see, e.g. figures 6, 7 and 9). This makes it challenging sometimes to numerically capture solutions of equation (1.1).

In this paper, we have implemented the second-order central-upwind semi-discrete scheme from [10, 12], which, for example, for equation (1.1), takes the form:

$$\frac{\mathrm{d}}{\mathrm{d}t}\bar{u}_j(t) = -\frac{H_{j+1/2}(t) - H_{j-1/2}(t)}{\Delta x} + \frac{P_{j+1/2}(t) - P_{j-1/2}(t)}{\Delta x}, \tag{B.1}$$

where the hyperbolic ($H_{j+1/2}$) and parabolic ($P_{j+1/2}$) fluxes are constructed as follows.

Let $x_\alpha = \alpha\Delta x$ be a uniform spatial grid, and $\bar{u}_j(t) \approx (1/\Delta x)\int_{x_{j-1/2}}^{x_{j+1/2}} u(x,t)\,\mathrm{d}x$ are computed cell averages at time t (for convenience, from now on we will omit the dependence of the computed quantities on t). We first reconstruct a piecewise linear approximation,

$$\tilde{u}(x,\cdot) = \bar{u}_j + s_j(x - x_j),$$

where the slopes s_j should be computed using a nonlinear limiter to avoid oscillations (for details, see [10]) and the references therein). This reconstruction is, in general, discontinuous at the cell interfaces, $x = x_{j+1/2}$, where it has two values, denoted by

$$u^-_{j+1/2} := \bar{u}_j + \frac{\Delta x}{2}s_j, \qquad u^+_{j+1/2} := \bar{u}_{j+1} - \frac{\Delta x}{2}s_{j+1}. \tag{B.2}$$

For a convex flux f, these discontinuities propagate in time with the one-sided local speeds that can be estimated by

$$a^-_{j+1/2} = \min\{|f'(u^+_{j+1/2})|, |f'(u^-_{j+1/2})|, 0\}, \qquad a^+_{j+1/2} = \max\{|f'(u^+_{j+1/2})|, |f'(u^-_{j+1/2})|, 0\}. \tag{B.3}$$

Finally, the numerical fluxes are

$$H_{j+1/2} = \frac{a^+_{j+1/2}f(u^-_{j+1/2}) - a^-_{j+1/2}f(u^+_{j+1/2})}{a^+_{j+1/2} - a^-_{j+1/2}} + \frac{a^+_{j+1/2}a^-_{j+1/2}}{a^+_{j+1/2} - a^-_{j+1/2}}(u^+_{j+1/2} - u^-_{j+1/2}), \tag{B.4}$$

and

$$P_{j+1/2} = \varphi(u_{j+1/2})Q\left(\frac{\bar{u}_{j+1} - \bar{u}_j}{\Delta x}\right), \qquad u_{j+1/2} := \frac{u^+_{j+1/2} + u^-_{j+1/2}}{2}. \tag{B.5}$$

The resulting semi-discretization (B.1)–(B.5) is a system of time-dependent ODEs that should be solved by a stable ODE solver of an appropriate order. To obtain an efficient fully

discrete method, we have used the explicit third-order large stability domain Runge–Kutta method, developed in [14, 15].

The strongly degenerate convection–diffusion equation (1.1) can be solved by several different methods. We have chosen to use the central-upwind scheme since it is a high-resolution shock capturing method, which can be applied to both hyperbolic and (degenerate) parabolic equations. When applied to convection–diffusion equations, this scheme has an additional advantage of not requiring an operator splitting, which allows one to completely avoid any splitting errors.

References

[1] Aronson D G 1970 Regularity properties of flows through porous media: the interface *Arch. Ration. Mech. Anal.* **37** 1–10

[2] Aronson D G, Caffarelli L A and Kamin S 1983 How an initially stationary interface begins to move in porous medium flow *SIAM J. Math. Anal.* **14** 639–58

[3] Barenblatt G I 1996 *Scaling, Self-Similarity, and Intermediate Asymptotics* (Cambridge: Cambridge University Press)

[4] Barenblatt G I 1952 On some unsteady motions of a liquid or a gas in a porous medium *Prikl. Mat. Mech.* **16** 67–78

[5] Bertsch M and Dal Passo R 1992 Hyperbolic phenomena in a strongly degenerate parabolic equation *Arch. Ration. Mech. Anal.* **117** 1–32

[6] Caffarelli L A and Friedman A 1979 Regularity of the free boundary for the one dimensional flow of gas in a porous medium *Am. J. Math.* **101** 1193–218

[7] Chertock A, Kurganov A and Rosenau P 2003 Formation of discontinuities in flux-saturated degenerate parabolic equations *Nonlinearity* **16** 1875–98

[8] Goodman J, Kurganov A and Rosenau P 1999 Breakdown in Burgers-type equations with saturating dissipation fluxes *Nonlinearity* **12** 247–68

[9] Kalashnikov A S 1967 Formation of singularities in solutions of the equation of nonstationary filtration *Z. Vychisl. Mat. i Mat. Fiz.* **7** 440–4

[10] Kurganov A, Noelle S and Petrova G 2001 Semi-discrete central-upwind schemes for hyperbolic conservation laws and Hamilton–Jacobi equations *SIAM J. Sci. Comput.* **21** 707–40

[11] Kurganov A and Rosenau P 1997 Effects of a saturating dissipation in Burgers-type equations *Commun. Pure Appl. Math.* **50** 753–71

[12] Kurganov A and Tadmor E 2000 New high-resolution central schemes for nonlinear conservation laws and convection–diffusion equations *J. Comput. Phys.* **160** 241–82

[13] Ladyženskaja O A, Solonnikov V A and Ural'ceva N N 1967 Linear and quasilinear equations of parabolic type *Trans. Math. Monographs* vol 23 (Providence, RI: American Mathematical Society)

[14] Medovikov A A 1998 High order explicit methods for parabolic equations *BIT* **38** 372–90

[15] Medovikov A A DUMKA3 code http://www.math.tulane.edu/∼amedovik

[16] Rosenau P *Diffusion Models with Saturated Diffusion* Unpublished manuscript

[17] Rosenau P 1990 Free energy functionals at the high gradient limit *Phys. Rev.* A **41** 2227–30

[18] Rosenau P, Hagan P, Northcutt R and Cohen D 1989 Delayed diffusion due to flux limitation *Phys. Lett.* A **142** 26–30

[19] Rykov Yu G 2000 Discontinuous solutions of some strongly degenerate parabolic equations *Russ. J. Math. Phys.* **7** 341–62